

Quantifying the reliability of four global datasets for drought monitoring over a semiarid region

Pari-Sima Katirai-Boroujerdy · Nasrin Nasrollahi ·
Kuo-lin Hsu · Soroosh Sorooshian

Received: 13 May 2014 / Accepted: 20 December 2014
© Springer-Verlag Wien 2015

Abstract Drought is one of the most relevant natural disasters, especially in arid regions such as Iran. One of the requirements to access reliable drought monitoring is long-term and continuous high-resolution precipitation data. Different climatic and global databases are being developed and made available in real time or near real time by different agencies and centers; however, for this purpose, these databases must be evaluated regionally and in different local climates. In this paper, a near real-time global climate model, a data assimilation system, and two gridded gauge-based datasets over Iran are evaluated. The ground truth data include 50 gauges from the period of 1980 to 2010. Drought analysis was carried out by means of the Standard Precipitation Index (SPI) at 2-, 3-, 6-, and 12-month timescales. Although the results show spatial variations, overall the two gauge-based datasets perform better than the models. In addition, the results are more reliable for the western portion of the Zagros Range and the eastern region of the country. The analysis of the onsets of the 6-month moderate drought with at least 3 months' persistence indicates that all datasets have a better performance over the western portion of the Zagros Range, but display poor performance over the coast of the Caspian Sea. Base on the results of this study, the Modern-Era Retrospective Analysis for Research and Applications (MERRA) dataset is a preferred alternative for drought analysis in the region when gauge-based datasets are not available.

P.-S. Katirai-Boroujerdy (✉)
Department of Meteorology, Faculty of Marine Science and
Technology, Tehran North Branch, Islamic Azad University, Tehran,
Iran
e-mail: sima_katirai@yahoo.com

N. Nasrollahi · K.-I. Hsu · S. Sorooshian
Center for Hydrometeorology and Remote Sensing (CHRS),
Department of Civil and Environmental Engineering, The Henry
Samueli School of Engineering, University of California, Irvine, CA,
USA

1 Introduction

Drought is a natural phenomenon that significantly impacts human life and activities (Wilhite et al. 2000). In contrast to floods, which are spatially and temporally limited extreme events, droughts usually affect extended areas over long periods of time. The Intergovernmental Panel on Climate Change (IPCC 2013) has reported that, over semiarid areas in mid and low latitudes, the mean annual river runoff and available water has decreased by 10–13 %, which increases the chance of drought and its impacts on these regions. To reduce vulnerability to drought, recent experiences have led governments to replace the traditional crisis management approach with a risk management approach (Grasso and Singh 2011). One of the most important elements in drought risk management is drought monitoring. Some developed countries have a capacity to monitor drought; however, many developing countries like Iran do not have adequate resources to provide drought-monitoring and early warning systems (Grasso and Singh 2011).

There are a few global and continental scale drought-monitoring systems, such as the U.S. Agency for International Development (USAID) African Drought Monitor, the University of Washington Experimental Surface Water Monitor, the Standardized Precipitation-Evapotranspiration Index Global Drought Monitor (Vicente-Serrano et al. 2010), the Global Drought Portal (GDP) by the United States National Climatic Data Center (Pozzi et al. 2013), and The Global Integrated Drought Monitoring and Prediction System (GIDMaPS, Hao et al. 2014), among others. Generally, global models are available in coarse resolutions with a time lag of a few months. Therefore, the majority of regional drought-monitoring systems rely on ground-based observations. In this respect, the main obstacle for drought monitoring in developing countries is the lack of access to high-quality climate information in near real time.

Usually, the lack of attention and low level of urgency given to the collection and processing of climate data from different ground-based stations causes a few years' delay in publishing the data. In addition, data gaps and irregular spatial coverage of stations in data-sparse regions reduce the quality of climate information, which leads to inhomogeneity of the datasets.

The primary variable of interest for drought monitoring is precipitation. Abnormal precipitation deficit leads to what is known as meteorological drought (McKee et al. 1993). The lack of high-quality and extensive long-term precipitation data is a major limitation for drought monitoring across remote and ungauged regions (AghaKouchak and Nakhjiri 2012). In recent years, remotely sensed products have provided new ways of monitoring precipitation from space (Sorooshian et al. 2000; Huffman et al. 2007; Hsu et al. 1997). The near real-time nature of remote-sensing datasets provides the opportunity to monitor precipitation across large spatial scales (Sorooshian et al. 2011). Several studies have integrated near real-time remote-sensing data and long-term datasets to generate near real-time observations for drought monitoring (AghaKouchak and Nakhjiri 2012). In addition to satellite observations, model simulations provide precipitation information for monitoring extremes, including the Global Land Data Assimilation System (GLDAS, Peters-Lidard et al. 2007) and the Modern-Era Retrospective Analysis for Research and Applications (MERRA, Reichle et al. 2011; Rienecker et al. 2011). These datasets can be used for various applications in different parts of the world (Mo 2008; Mo et al. 2011; Yi et al. 2011; Hao et al. 2014; Livneh et al. 2010; Fox and Rowntree 2013). For example, MERRA data has been used in many regional drought studies across the world (e.g., AghaKouchak 2014a, b). However, they have not been evaluated against ground-based observations over Iran.

These products differ in numerous ways because of different processes of construction. Prior to the use of different datasets, their quality must be evaluated over different climatic and geographic regions of the world (Dinku et al. 2010; Kidd et al. 2012; Barlow et al. 2006). However, the evaluation of these land-atmospheric models has generally been limited to the USA and other observation-rich regions of the world (Kim et al. 2014), even though one of their promised strengths is in their ability to provide information on land surface processes in data-poor regions. Such analysis will give better guidance to users in selecting a product for their particular application and will help model producers to improve the accuracy of model parameter fields, meteorological forcing, and various physical processes.

Historically, Iran has suffered from significant droughts. In a recent study, Damberg and AghaKouchak (2014) showed that the precipitation of northwestern and eastern Iran exhibits a drying trend. Numerous studies have been conducted on drought in Iran (Mirabbasi et al. 2014; Sayari et al. 2013;

Tabari et al. 2012, 2013; Hosseinzadeh Talaei et al. 2014), but only a few of them address the evaluation of global datasets for drought monitoring. Rahimzadeh Bajgiran et al. (2008) evaluated the National Oceanic and Atmospheric Administration (NOAA)-AVHRR data for drought monitoring in northwestern Iran. They calculated the correlation coefficient between the Normalized Difference Vegetation Index (NDVI) and the Vegetation Condition Index (VCI) to precipitation (observation data) for 5 years of data. Their results showed that the NDVI correlates well with precipitation variation in the study area. Razinei et al. (2009) applied the principal component analysis (PCA) to a 12-month Standard Precipitation Index (SPI) time series derived from a gauge-based dataset and to the National Centers for Environmental Prediction/National Center for Atmospheric Research (NCEP/NCAR) precipitation dataset for western Iran for the period 1966–2000. They found two distinct subregions (in the northwest and southwest areas of the country) with different climatic variability, which showed satisfactory agreement between the two datasets. Razinei et al. (2011) applied the PCA to a 12-month SPI time series using the Global Precipitation Climatology Center (GPCC) and NCEP/NCAR precipitation datasets for drought analysis over the entire country for the period 1951–2005 and checked the results against 32 rain gauges. Their results showed subregions of drought variability that are in agreement with ground observations. However, the time variability of the NCEP/NCAR-rotated PC scores associated with those subregions was different from GPCC and ground observations. They also concluded that the NCEP/NCAR dataset shows better agreement with observations for the period 1970–2005 than for 1951–2005. Golian et al. (2014) studied the trend and characteristics of meteorological and agricultural droughts in different conditions in Iran. Their results show that there is a positive significant drought trend in the northern and central parts of Iran, while the eastern parts did not experience any significant trend. They also studied the most severe drought that occurred between 1998 and 2001 and showed that this event coincided with a prolonged cold phase, namely the El Niño-Southern Oscillation.

The objective of this paper is to perform an evaluation and comparison of real-time global model-based reanalysis precipitation dataset from MERRA, GLDAS, and two global and continental gauge-based gridded datasets for drought monitoring over Iran. GPCC provides the global gauge-based gridded dataset. GPCC data is based on the rational merging of data series from rain gauges built from the Global-Telecommunication-System-based data and historic data records, from a worldwide total of more than 67,000 stations (Schneider et al. 2014). The Asian Precipitation—Highly-Resolved Observational Data Integration Towards Evaluation (APHRODITE, Yatagai et al. 2012) is a daily gridded precipitation dataset created by collecting rain gauge

observation data across Asia. The product contributes to studies such as the evaluation of Asian water resources and has different interpolation methods. The datasets used in this study will be described in detail in Section 3.

2 Study area

Iran is located in the arid and semiarid parts of the subtropical latitudes of the Northern Hemisphere and has different climate regions (Fig. 1). The most central part of the country is covered by deserts. The negative water balance is the consequence of the lack of summer precipitation with high evapotranspiration in this area. Water is often scarce in the region and the management of water resources is a priority. The complex topography, which includes the Zagros Range (in the western section) and the Alborz Range (in the northern section), plays a key role in influencing precipitation patterns over the country. The central part of Iran is usually isolated from the humid air masses by these mountain ranges. The annual precipitation varies from less than 50 mm in the southeast to more than 1600 mm in the north (the coast of the Caspian Sea).

3 Data

Four different precipitation datasets are used in this study: one near-real time global model-based reanalysis precipitation dataset (MERRA), one land data assimilation product (GLDAS), and two gridded gauge-based datasets (GPCC and APHRODITE).

MERRA product has been designed to support the National Aeronautics and Space Administration (NASA)'s earth science research interests by producing a global long-term dataset for the satellite era from 1979 to the present (Rienecker et al. 2011). It incorporates Earth Observing System satellite-based observations into a climate context to improve the hydrologic cycle represented in earlier generations of reanalysis. MERRA has been developed by the NASA's Global Modeling and Assimilation Office. MERRA land surface estimates reflect the time integration of surface meteorological conditions (precipitation, radiation, wind speed, etc.) by the short-range model forecast accumulations. The GEOS-5 data assimilation system used for MERRA implements the incremental analysis updates (IAU) to slowly adjust the model states towards the observed states. MERRA estimates of surface meteorological and land surface fields are available at hourly time steps and at $1/2^{\circ} \times 2/3^{\circ}$ resolution in

Fig. 1 The study area



latitude and longitude, respectively (Rienecker et al. 2011; Reichle et al. 2011).

GLDAS has been developed jointly by NASA, the Goddard Space Flight Center (GSFC), the NOAA, and the NCEP. GLDAS makes use of the new generation of ground- and space-based observation systems, which provide data to constrain the modeled (CLM, Mosaic, Noah, and VIC) land surface states. The U.S. Naval Research Laboratory (NRL) near-real-time satellite-derived precipitation product (Turk et al. 2000) is one of the precipitation-forcing datasets with the spatial resolution of 0.25° and a temporal resolution of 6 h covering the area from 60° S to 60° N. Another precipitation forcing option that is being tested makes use of the global 2.5° 5-day NOAA Climate Prediction Center (CPC)'s Merged Analysis of Precipitation (CMAP), which is a blending of satellite and gauge observations. These precipitation fields are aggregated spatially and temporally to match the GLDAS resolutions. Current data holdings include a set of 1.0° resolution data products from the models (Rodell et al. 2004).

The GPCP (Schneider et al. 2011) performs analyses of the global land surface precipitation distribution. Its main task is the analysis of monthly precipitation for the Earth's land surface on the basis of rain gauge (in situ) measurements. GPCP's database comprises precipitation data mainly on a monthly basis from a variety of sources. GPCP's new global precipitation climatology datasets are available in different spatial resolutions. The $0.5^\circ \times 0.5^\circ$ longitude-by-latitude resolution (V6 full data nobs 1901–2010) is used in this study (Schneider et al. 2014).

For Asia, the APHRODITE project of water resources has developed daily precipitation datasets with high-resolution grids. The datasets are created primarily with data obtained from a rain gauge observation network (Yatagai et al. 2012). This dataset is available in 0.5° spatial resolution.

In this paper, we use the general name of “model datasets” for the GLDAS and MERRA products and “gauge-based datasets” for GPCP and APHRODITE datasets. For the period 1980–2010 (except for APHRODITE, which is 1980–2007), the daily precipitation was accumulated to a monthly scale for all datasets over Iran (between 25° N– 40° N and 44° E– 64° E).

The reference data are from 50 quality-controlled synoptic stations operated by the Iranian Meteorological Organization (IMO) for the period 1980–2010. It is likely that the GPCP and APHRODITE analysis systems have used these data for bias adjustment, as mentioned above. Only a few stations had one or two monthly precipitation estimates missing in the study period. The missing data were substituted with the mean monthly value over the study period.

4 Methods

4.1 The Standard Precipitation Index

The most essential key for drought analysis and monitoring is to select an appropriate drought indicator. The SPI (McKee et al. 1993) has been recommended by the World Meteorological Organization (WMO) as the reference drought index. Although SPI is used to estimate drought, it identifies both nonnormal dry and humid periods. Moreover, it allows the analysis of droughts at different temporal scales (Edwards and McKee 1997).

The gamma distribution is commonly used to compute the cumulative probability distribution of the long-term monthly precipitation record. It is then transformed into the inverse of the standard normal distribution (McKee et al. 1993). In addition to gamma distribution, different distribution functions were also used for calculating SPI (Guttman 1999; Vicente-Serrano 2006; Hao and AghaKouchak 2013). Following Hao and AghaKouchak (2014), an empirical probability described by Gringorten (1963) is used in this paper to calculate the SPI. Based on SPI values, dry and wet periods were divided into 11 categories (Table 1).

4.2 Spearman rank correlation coefficient

In this study, the Spearman rank correlation coefficient, which is a nonparametric measure of statistical dependence between two variables (SPI series of the gauge-reference dataset and the four selected datasets), is used, because it excludes the effect of marginal values and shows the strength of the associations between the two variables. The Spearman coefficient, r_s , is the correlation coefficient of the linear regression between the ranked variables and is obtained from the expression:

$$r_s = 1 - \frac{6 \sum d_i^2}{N(N^2 - 1)} \quad (1)$$

where N is the number of data items in the series, and d is the difference in statistical rank of corresponding variables. In order to examine whether the null hypothesis (that there is no

Table 1 Dry/wet conditions categorized according to the SPI value

SPI	Classification	SPI	Classification
0 to -0.49	Near normal	0 to +0.49	Near normal
-0.5 to -0.7	Abnormally dry	+0.5 to +0.7	Abnormally wet
-0.8 to -1.2	Moderately dry	+0.8 to +1.2	Moderately wet
-1.3 to -1.5	Severely dry	+1.3 to +1.5	Severely wet
-1.6 to -1.9	Extremely dry	+1.6 to +1.9	Extremely wet
<-2	Exceptionally dry	>+2	Exceptionally wet

association) can be rejected or not, it is necessary to calculate the probability, which is calculated using a table of reduced normal distribution. If

$$\alpha = P(|u| > |u(r_s)|), \text{ with } u(r_s) = r_s(N-1)^{1/2} \quad (2)$$

$\alpha < \alpha_0$, the null hypothesis is rejected for a significance level of α_0 . If a trend is detected, it will be an increasing or decreasing trend, depending on whether $r_s > 0$ or $r_s < 0$ (del Rio et al. 2005). The comparison between different datasets and the reference gauge data's SPI was performed using the Spearman correlation for every selected pixel.

4.3 Critical Success Index

To determine how well drought could be detected, the Critical Success Index (CSI) is defined as the portion of the correct drought detections by each dataset. If a drought event is estimated by using the dataset's SPI, the SPI of the gauge verifies the occurrence of the drought. The scoring techniques applied here consider the following quantities for any given SPI threshold: Z , the number of correct monitoring of nonoccurrence; F , the number of false alarms or wrong monitoring; M , the number of misses or nondetected events; and H , the number of hits or correct drought monitoring. The total monitoring number (gauge SPIs) is then defined as $N = Z + F + M + H$. In this study, the $SPI = -0.5$, which is considered as the threshold for drought events (Wilks 2006):

$$CSI = H / (F + M + H) \quad (3)$$

The selected datasets are available in different spatial resolutions. The resolutions of MERRA, GLDAS, GPCC, and APHRODITE data are $1/2^\circ \times 2/3^\circ$, $1^\circ \times 1^\circ$, $0.5^\circ \times 0.5^\circ$, and $0.5^\circ \times 0.5^\circ$, respectively. In case there is a specific grid, the arithmetic mean of the gauge data is used for the pixel. Based on collocated gauge and gridded data, 46 pixels of MERRA, 40 pixels of GLDAS, and 48 pixels of GPCC and APHRODITE are considered. The 2-, 3-, 6-, and 12-month SPIs are calculated for the above four datasets and also for the reference gauge data.

5 Results

To evaluate the performance of the four precipitation datasets over Iran, the SPI is calculated for 2-, 3-, 6-, and 12-month timescales at each grid point (which includes at least one gauge). Then, the Spearman correlations for the SPI series versus the gauge data in the selected pixels are calculated. Table 2 shows the mean correlation coefficients of the 2-, 3-, 6-, and 12-month SPIs between the gauge reference data and

Table 2 Mean correlation coefficients between reference gauge data and selected datasets for the 2-, 3-, 6-, and 12-month SPIs

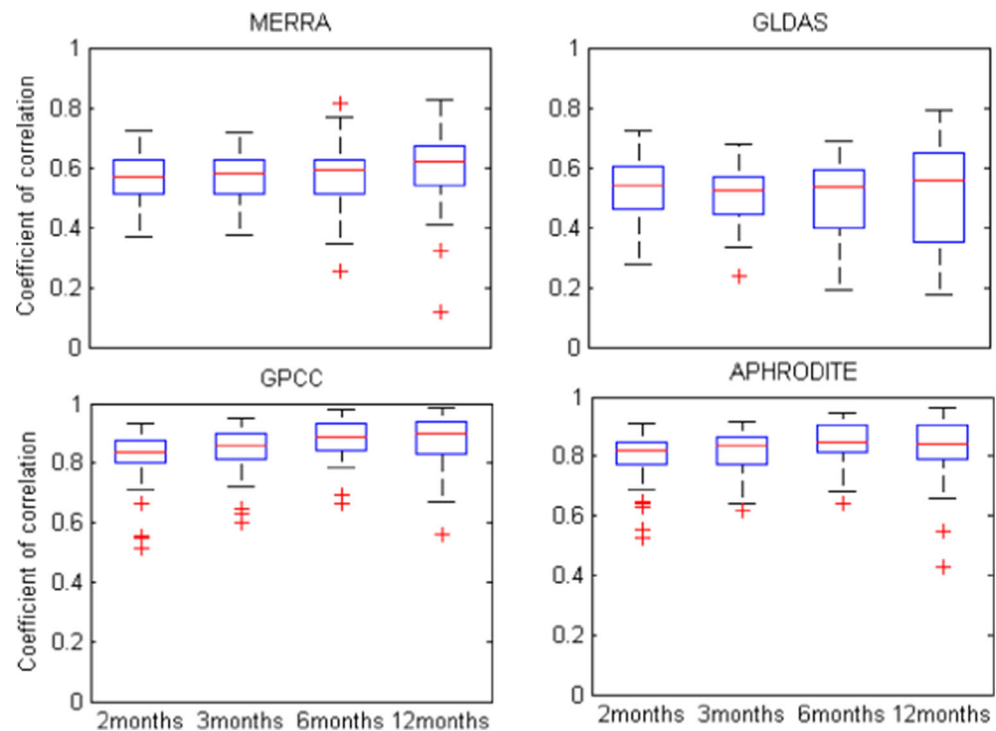
Month SPI	Gauge-based datasets		Global model datasets	
	GPCC	APHRODITE	MERRA	GLDAS
2	0.80	0.80	0.57	0.58
3	0.84	0.82	0.58	0.55
6	0.90	0.86	0.62	0.53
12	0.91	0.86	0.64	0.53
Number of grid cells	48	48	46	40

the four selected datasets. It must be noted that these results show only the mean temporal correlations between compared data series. The lower number of GLDAS grid cells is due to low spatial resolution and the lack of data in some islands in the Persian Gulf from this land surface model. The results show that, in general, correlation coefficients increase when increasing the SPI timescale for all datasets, but not for GLDAS. Maybe these results for GLDAS is due to lower spatial resolution that reduces the accuracy in estimating precipitation in each pixel when we compare with gauges which are point scale measurements. So the accumulation of these errors leads to worst results when SPI time period increases.

Figure 2 represents the box plots of the correlation (over all selected grid cells) as a function of the SPI time. The results show that the two gauge-based products (GPCC and APHRODITE), when compared to the model-generated datasets (MERRA and GLDAS), have very high scores, which increase as the timescale increases. The bar line in each box shows the median of the data. The results for GPCC are slightly better than the results for APHRODITE. On the other hand, the global models show poor correlations, especially for shorter timescales. The MERRA correlations are slightly greater, especially for GLDAS' 12-month SPIs. Although the median of correlations for GPCC and APHRODITE are above 0.8, there are correlations as low as 0.5 (+ sign in the figure), indicating the considerable differences between compared datasets in some of the pixels.

The spatial pattern of drought over Iran is very complex. The western and eastern parts of the country have different climate regimes and sometimes observed to have reverse dry and wet periods. This situation is not unique to Iran and has been reported in other parts of the world (Madadgar and Moradkhani 2013; Nkemdirim and Weber 1999; Oladipo 1995; Fowler and Kilsby 2002, among others). Different wet and dry periods in the eastern versus western areas are attributed to complicated circulation patterns that are predominant in regions located in subtropical climatic transition areas, such as Iran. The inverse temporal variations of 6-month SPIs for two pixels located in eastern and western Iran show that the

Fig. 2 Box plots summarizing the evaluation results for the temporal correlation between the reference gauge dataset and four datasets (MERRA, GLDAS, GPCC, and APHRODITE). Correlation coefficients are averaged over all selected grid points over Iran. The *red line* shows the median of quantities. *Box*: 25th and 75th percentiles; *whiskers*: 10th and 90th percentiles; *+* show the maximum and minimum values



dryness in the west occasionally coincides with a wet period in the east, and vice versa (Fig. 3). Actually, the western section of the country is primarily affected by Mediterranean lows from the west and Sudan lows from the southwest, and the majority of annual precipitation falls in winter and spring, while the summer is dry. On the other hand, the eastern part of Iran is mostly dry, with less than 50 mm of annual precipitation. However, summer monsoons may affect the area by providing a large amount of daily precipitation. Therefore, to have a reliable drought-monitoring system for the entire country, the regional differences should be considered.

Figure 4 shows the spatial pattern of correlations between 3-month SPIs based on reference gauge data and four selected datasets. It is not surprising that the gauge-based datasets (GPCC and APHRODITE) are superior in capturing the SPI temporal variations, with average correlations of above 0.8. Similar results are represented in Fig. 2 for the average correlation value. The correlations in the area west of the Zagros Range were found to be better than other parts of the area for all datasets. In comparison, between the two global model-generated datasets (MERRA and GLDAS), MERRA shows a slightly better performance.

Fig. 3 The time series of reference gauge data 6-month SPI for a pixel in western (*red*) and eastern (*blue*) Iran for the study period

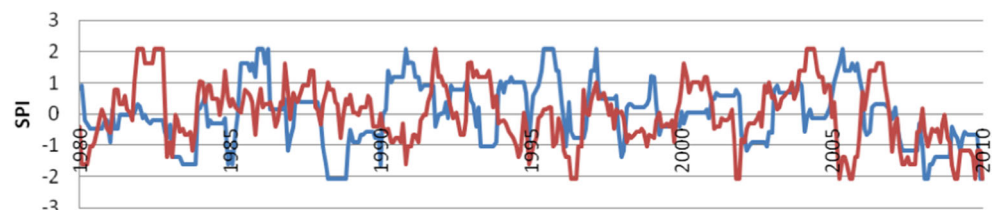
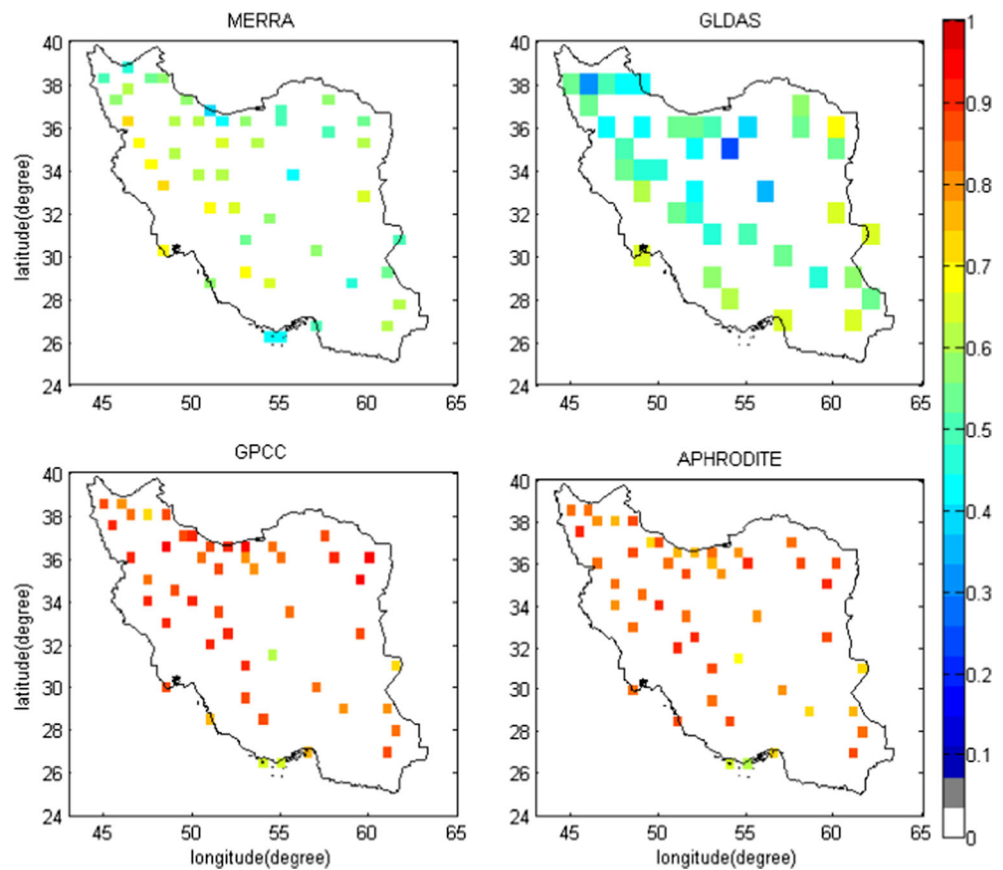


Figure 5 represents the correlations for 12-month SPIs. It is shown that, overall, the correlations for almost all datasets tend to be higher for longer (12-month) timescales compared to shorter (3-month) timescales. GLDAS shows lower correlations for the north and central parts of the country when the SPI timescale increases.

However, all datasets show higher correlations for grid cells at the coast of the Persian Gulf as the SPI timescale increases; nevertheless, at the coast of the Caspian Sea, correlations decrease when the timescale increases. The aforementioned problem could be related to the accumulation of errors in the coast of the Caspian Sea, as discussed in Katirai-Boroujerdy et al. (2013).

As mentioned above, for the entire country of Iran, except for a narrow strip over the coast of the Caspian Sea and a small area in the southeastern section of the country, which have summer rainfall, the largest portion of annual precipitation occurs in a 6-month period (primarily winter and spring). Thus, the small amount of precipitation (which is negligible) in other months causes a considerable variation in SPIs. Occasionally, these small amounts of precipitation are not captured by the models, and therefore, the correlations can

Fig. 4 Spatial distribution of temporal correlation coefficients between the 3-month SPI gauge dataset and MERRA, GLDAS, GPCC, and APHRODITE



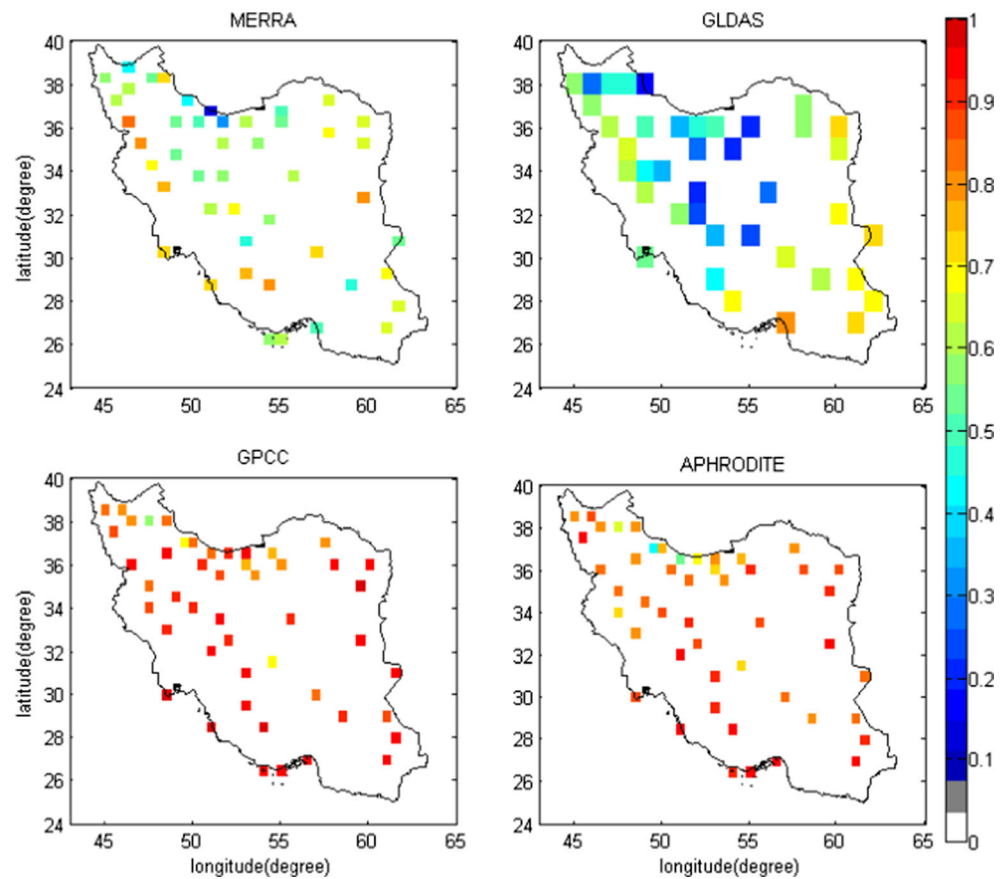
be reduced considerably. Therefore, the 6-month SPIs for the six wet months (November–April) for selected pixels are considered, and the correlation coefficients are calculated. The average of correlations for GPCC, APHRODITE, MERRA, and GLDAS are 0.93, 0.88, 0.67, and 0.59, respectively. The wet season correlations show better agreements with observations in comparison to the wet and dry season results (Table 2) for all datasets.

To demonstrate how well each dataset can monitor drought, the CSI is calculated for the datasets and for the 2-, 3-, 6-, and 12-month periods. Table 3 shows the mean CSIs over the selected pixels for various SPIs. The result shows that GPCC and APHRODITE captured the dry periods better than the two others for all timescales. Maximum CSIs were approximately 58–69 % for the 2- to 12-month SPIs for GPCC, and minimum CSIs were ~36–40 % for the 12- to 2-month SPIs for GLDAS data. GLDAS is the only dataset that has higher CSI values at shorter timescales. Actually, GLDAS data is more erroneous in comparison with other datasets.

Figure 6 gives the box plots of the mean CSI (over all selected grid cells) as a function of the SPI timescale. This figure also illustrates that the GPCC shows the best performance and GLDAS has the poorest. The CSI values are not as good as the correlations (Fig. 2).

Figure 7 shows the spatial pattern of CSIs (in percentages) of monitoring dry periods for all datasets based on reference gauge data as a function of timescale. Confirming the previous results, Fig. 7 illustrates that the GPCC and APHRODITE reveal dry periods better than the global model datasets, due to the fact that these datasets use the reference gauge data. The GPCC has better performance than APHRODITE. The results show that the dry period prediction by MERRA is more reliable than the prediction given by GLDAS. However, the CSIs of GLDAS over the eastern and southeastern areas are found to be slightly better as the timescale increases; they decrease with timescale over the central and northern portions of the area. The dry period prediction skill by MERRA over the coast of the Caspian Sea decreases as the timescale increases. It should be noted that the CSI increase in the southern parts of the country, especially over a region from southwest to east, is shown in Fig. 7 (perpendicular to the Zagros Range). The GPCC and APHRODITE give poor results over the southern part of the country (the Hormoz Strait) for short timescales, which improves as the timescale increases. On the other hand, APHRODITE, which captures the dry periods adequately in the northern section of the country, gets worse when the timescale increases.

Droughts develop slowly and have impacts on a region once water shortage occurs. Hence, not only is the duration of

Fig. 5 Same as Fig. 4, but for 12-month SPIs

the drought very important for a variety of applications, so is the detection, especially for decision making and water management. Because most parts of the country are affected by the 6-month wet period, the 6-month SPI for the moderate dry category with at least 3 months in duration is selected to evaluate the ability of different datasets in recognizing drought onset. A drought lasting longer than 3 months was chosen because a duration of more than that time frame in a year can cause serious damages in different sectors (water management, agriculture, etc.). Figure 8 shows how well (by percentages) each dataset can detect the onset of 6-month moderate droughts with durations of at least 3 months. All datasets show better performance over the area west of the Zagros Range. On the other hand, almost all datasets (except GPCC) demonstrate

poor results for the coast of the Caspian Sea. The gauge-based datasets superiorly monitor drought onset over all regions. Comparing the southern half of Iran to the northern half, GLDAS shows better detection performance over the southern part. MERRA detected the onset of moderate droughts with a detection rate between 16 and 85 %. Although APHRODITE can detect the onset of a drought in most grid cells (between 25 and 100 %), it is unsuccessful in the western area of the Caspian Sea. GPCC has the best score (between 40 and 100 %) in comparison with the other products.

6 Conclusion

The reliability of precipitation information from two gauge-based (GPCC and APHRODITE) databases and two model-generated global datasets (MERRA and GLDAS) for hydroclimatological monitoring, especially drought, is examined and quantified over Iran. The study area includes semi-arid and hyperarid regions where these datasets have not been evaluated for drought monitoring. The “ground truth” is from the quality-controlled Iranian Meteorological Organization gauge dataset, which includes 50 long-term records. The time period of 1980–2010 is considered for the analysis, except for APHRODITE, for which data are only available until 2007.

Table 3 The mean CSI (%) over the selected pixels for different datasets

CSI (%)	2-month SPI	3-month SPI	6-month SPI	12-month SPI
MERRA	39.9	41.1	43.7	45.1
GLDAS	39.6	37.6	38	36.3
GPCC	58.2	60.3	68.1	69.4
APHRODITE	54.3	57	62.3	61.4

Fig. 6 Box plot of the CSI mean (over selected grid cells) as a function of SPI timescale for the four datasets (MERRA, GLDAS, GPCC, and APHRODITE). Again, the red line shows the median of quantities. Box: 25th and 75th percentiles; whiskers: 10th and 90th percentiles; + show the maximum and minimum values

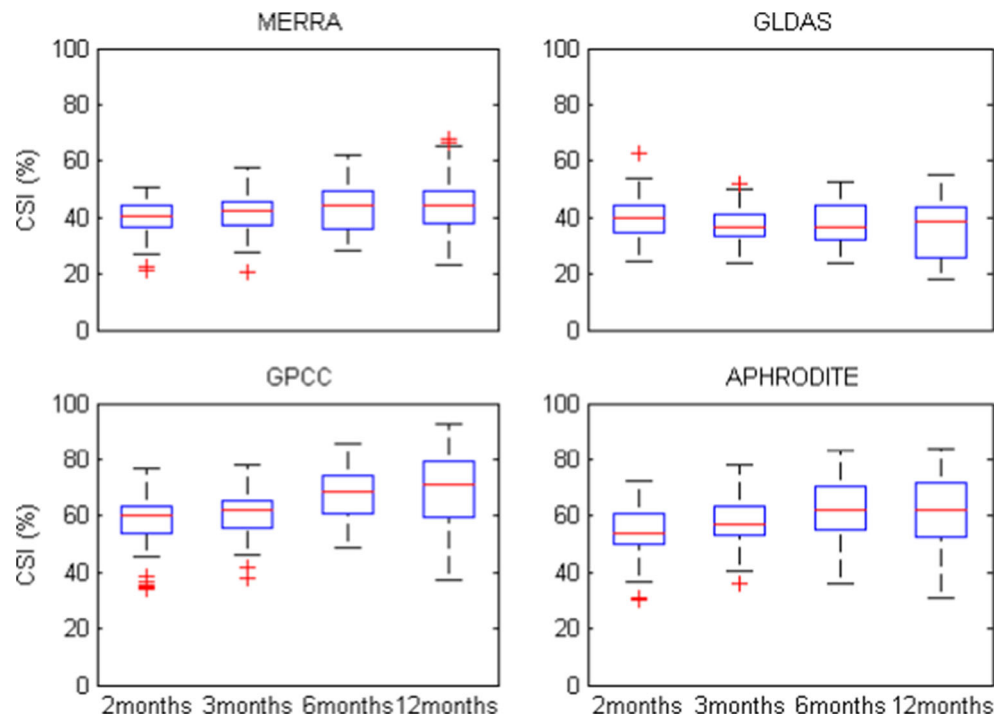


Fig. 7 The spatial distribution of the CSI for all datasets as a function of SPI timescales

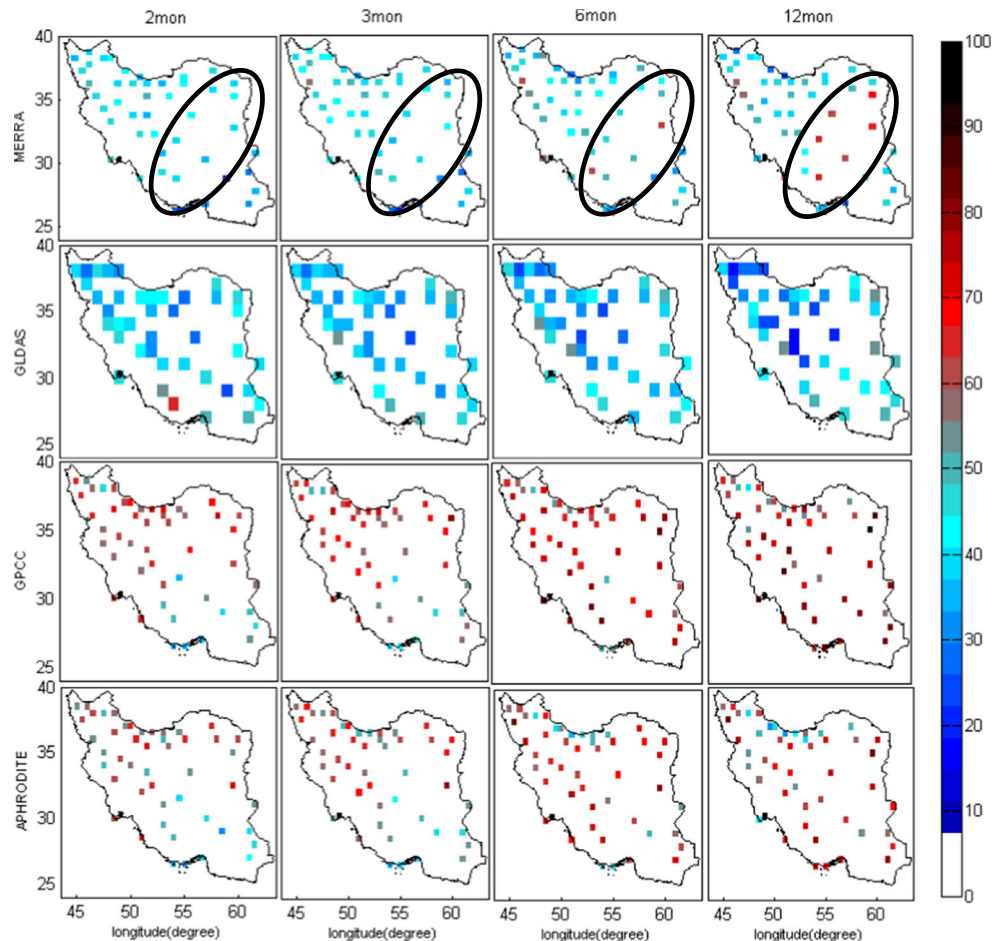
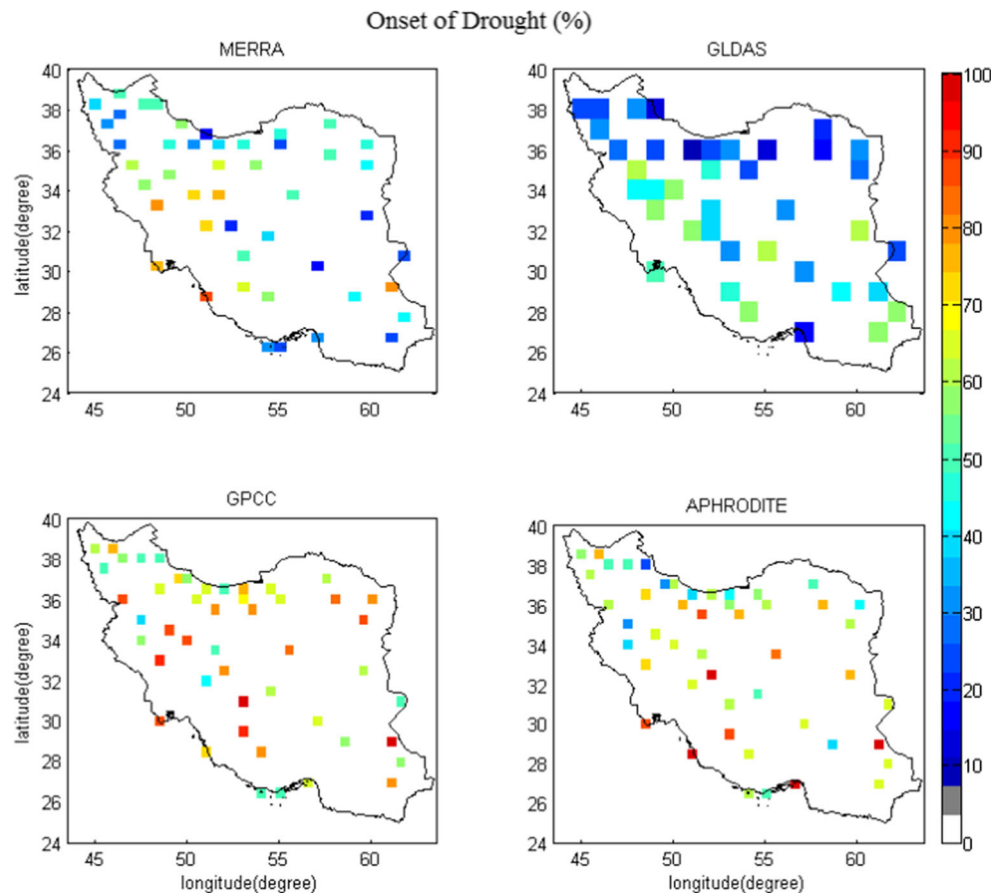


Fig. 8 Detection of the 6-month moderate dry onset with a persistency of at least 3 months (in percent)



The 2-, 3-, 6-, and 12-month SPIs are calculated to assess drought conditions in selected pixels. In addition, the comparison among different datasets and reference gauge data was performed using the Spearman rank correlation for selected pixels. As one expects, the results indicate that the two gauge-based products (GPCC and APHRODITE) show superior scores compared to the global model datasets (MERRA and GLDAS). The performance score improves as the timescale increases. The maximum mean correlation (for the selected pixels) for the 12-month SPI is 0.91 for GPCC, and the minimum mean correlation is 0.53 for GLDAS. On the other hand, the global models show poor correlations, especially for shorter timescales. The spatial patterns of correlations in the west of the Zagros Range were found to be better than in other parts of the region for all datasets. GLDAS shows lower correlations for the north and central parts of the country when the SPI timescale increases. On the other hand, all datasets show higher correlations for grid cells on the coast of the Persian Gulf as the SPI timescale increases. The precipitation records show that Iran's climate is dominated mostly by precipitation in the winter and spring months. Therefore, the 6-month SPIs for the six wet months of the year (November–April) are considered. The averages of wet season correlations improved in comparison with all data results, and the results were consistent in all data products.

To show the performance of the datasets for drought monitoring, the CSI is calculated for the 2-, 3-, 6-, and 12-month periods with the gauge dataset as a reference. The results show that GPCC and APHRODITE captured the dry periods better than the two other datasets for all timescales. GLDAS is the only dataset that the CSI values do not improve when timescales increase. The results show that the dry period prediction by MERRA is more reliable than that by GLDAS. Although the CSIs of GLDAS over the eastern and southeastern areas are slightly greater in comparison with other parts of the country, they decrease with increasing timescales over the center and northern regions. The CSIs of MERRA increase in the southern parts of the country, especially over a region from the southwest to the east, perpendicular to the Zagros Range as the timescale increases. It seems that this needs more investigations. GPCC and APHRODITE give poor results over the southern portion of the country (the Hormoz Strait) for short timescales, but the results improve as the timescale increases. However, APHRODITE shows different results in the northern section of Iran, where it captures dry periods adequately in short timescales but shows lower performance when the timescale increases. In addition, the detection of the onsets of 3 months of persistent, moderate droughts for each dataset was compared with the gauge data. The results show that all datasets have better performance west of the Zagros

Range, but poor performance over the coast of the Caspian Sea. It should be noted that the superior performance of gauge-based datasets is likely to be influenced by the fact that some of the gauges from the IMO used in this study are also the gauges whose data has been used in the GPCC. In the southern half of the country, GLDAS has better performance than in the northern half. It is worth mentioning that the regional differences in the performance of various datasets are highlighted here and need further investigations. As mentioned earlier, the objective of the present study is the evaluation and comparison of various gridded based global precipitation datasets for drought monitoring over Iran. The quality of each dataset depends on many factors such as interpolation techniques, sources of data, availability of ground-based dataset, and grid resolution, among others. This study shows better performance of the GPCC dataset in general; however, more studies are required to investigate the differences among the datasets and the reason for the performance variations that is beyond the objectives of this study.

As shown in this paper, the GPCC is able to show the dry and wet periods reasonably well from 2- to 12-month time-scales. Unfortunately, this dataset is not available in near real time (currently, GPCC data are available with a delay of approximately 2 years). If near real-time analysis is not critical, we suggest that the GPCC is the best reference dataset for long-term historical climate studies. However, for near real-time drought analysis, the GPCC data is not suitable due to its latency. On the other hand, MERRA is a reasonable alternative for near real-time drought analysis and prediction over Iran when GPCC or other gauge-based datasets are not available. However, the MERRA data does not exhibit good performance over the coast of the Caspian Sea.

References

- AghaKouchak A, Nakhjiri N (2012) A near real-time satellite-based global drought climate data record. *Environ Res Lett*. doi:10.1088/1748-9326/7/4/044037
- AghaKouchak A (2014a) A multivariate approach for persistence-based drought prediction: application to the 2010–2011 East Africa drought. *J Hydrol*. doi:10.1016/j.jhydrol.2014.09.063
- AghaKouchak A (2014b) A baseline probabilistic drought forecasting framework using standardized soil moisture index: application to the 2012 United States drought. *Hydrol Earth Syst Sci* 18:2485–2492. doi:10.5194/hess-18-2485-2014
- Barlow M, Cullen H, Lyon B, Wilhelmi O (2006) Drought disaster in Asia. *Nat Disaster Hotspots Case Stud* 6:1–20
- Damberg L, AghaKouchak A (2014) Global trends and patterns of droughts from space. *Theoret Appl Clim* 117:441–448
- del Rio S, Penas A, Fraile R (2005) Analysis of recent climatic variations in Castile and Leon (Spain). *Atmos Res* 73:69–85
- Dinku T, Connor SJ, Ceccato P (2010) Comparison of CMORPH and TRMM-3B42 over mountainous regions of Africa and South America, In *Satellite rainfall applications for surface hydrology*. Springer, Netherlands, pp 193–204. doi:10.1007/978-90-481-2915-7-11
- Edwards EC, McKee TB (1997) Characteristics of 20th century drought in the United States at multiple time scales, *Climatology Rep*. 97–2, Atmospheric Science Paper 634, Department of Atmospheric Science, Colorado State University, Fort Collins, CO, 155 pp, Available online at <http://ccc.atmos.colostate.edu/edwards.pdf>
- Fowler HJ, Kilsby CG (2002) A weather-type approach to analyzing water resource drought in the Yorkshire region from 1881–1998. *J Hydrol* 262:177–192
- Fox RC, Rowntree KM (2013) Extreme weather events in the Sneeuweberg, Karoo, South Africa: a case study of the floods of 9 and 12 February 2011. *Hydrol Earth Syst Sci Discuss* 10:10809–10844
- Golian S, Mazdiyasi O, AghaKouchak A (2014) Trends in meteorological and agricultural droughts in Iran. *Theoret Appl Clim*. doi:10.1007/s00704-014-1139-6
- Grasso VF, Singh A (2011) Early warning systems: state-of-art analysis and future directions. Draft report, UNEP, (Available online at https://na.unep.net/siouxfalls/publications/Early_Warning.pdf)
- Gringorten II (1963) A plotting rule for extreme probability paper. *J Geophys Res* 68:813–814
- Guttman NB (1999) Accepting the standardized precipitation index: a calculation algorithm JAWRA. *J Am Water Resour Assoc* 35:311–322
- Hao Z, AghaKouchak A (2013) Multivariate standardized drought index: a parametric multi-index model. *Adv Water Resour* 57:12–18
- Hao Z, AghaKouchak A (2014) A nonparametric multivariate multi-index drought monitoring framework. *J Hydrometeorol* 15:89–101
- Hao Z, AghaKouchak A, Nakhjiri N, Farahmand A (2014) Global integrated drought monitoring and prediction system. *Sci Data*. doi:10.1038/sdata.2014.1
- Hosseinzadeh Talaee P, Tabari H, Sobhan Ardakani S (2014) Hydrological drought in the west of Iran and possible association with large-scale atmospheric circulation patterns. *Hydrol Process* 28:764–773
- Hsu K, Gao X, Sorooshian S, Gupta HV (1997) Precipitation estimation from remotely sensed information using artificial neural networks. *J Appl Meteorol* 36:1176–1190
- Huffman G, Adler R, Bolvin D, Gu G, Nelkin E, Bowman K, Stocker E, Wolff D (2007) The TRMM multi-satellite precipitation analysis: quasi-global, multiyear, combined sensor precipitation estimates at fine scale. *J Hydrometeorol* 8:38–55
- IPCC (2013) In: Stocker TF, Qin D, Plattner G-K, Tignor M, Allen SK, Boschung J, Nauels A, Xia Y, Bex V, Midgley PM (eds) *Climate Change 2013: The physical science basis*. Contribution of Working Group I to the Fifth Assessment Report of the Intergovernmental Panel on Climate Change. Cambridge University Press, Cambridge. doi:10.1017/CBO9781107415324, 1535 pp
- Katiraei-Boroujerdy PS, Nasrollahi N, Hsu KL, Sorooshian S (2013) Evaluation of satellite-based precipitation estimation over Iran. *J Arid Environ* 97:205–219
- Kidd CP, Bauer J, Turk G-J, Huffman R, Joyce K-L, Hsu K, Braithwaite D (2012) Intercomparison of high-resolution precipitation products over Northwest Europe. *J Hydrometeorol* 13:67–83
- Kim CJ, Park MJ, Lee JH (2014) Analysis of climate change impacts on the spatial and frequency patterns of drought using a potential drought hazard mapping approach. *Int J Climatol* 34:61–80
- Livneh B, Xia Y, Mitchell KE, Ek MB, Lettenmaier DP (2010) Noah LSM snow model diagnostics and enhancements. *J Hydrometeorol* 11:721–738
- Madadgar S, Moradkhani H (2013) Drought analysis under climate change using copula. *J Hydrol Eng* 18(7):746–759
- McKee TB, Doesken NJ, Kleist J (1993) The relationship of drought frequency and duration to time scales, preprints, Eighth Conf. on Applied Climatology, Anaheim, CA, Amer. Meteor. Soc., 179–184

- Mirabbasi R, Anagnostou EN, Fakheri-Fard A, Dinpashoh Y, Eslamian S (2014) Analysis of meteorological drought in northwest Iran using the Joint Deficit Index. *J Hydrol* 492:35–48
- Mo KC (2008) Model-based drought indices over the United States. *J Hydrometeorol* 9:1212–1230
- Mo KC, Long LN, Xia Y, Yang SK, Schemm JE, Ek M (2011) Drought indices based on the climate forecast system reanalysis and ensemble NLDAS. *J Hydrometeorol* 12(2):181–205
- Nkemdirim L, Weber L (1999) Comparison between the droughts of the 1930s and the 1980s in the southern prairies of Canada. *J Clim* 12: 2434–2450
- Oladipo EO (1995) Some statistical characteristics of drought area variations in the savanna region of Nigeria. *Theoret Appl Clim* 50:147–155
- Peters-Lidard C, Houser PR, Tian Y et al (2007) High-performance Earth system modeling with NASA/GSFC's land information system, *Innovations Syst. Softw Eng* 3:157–165
- Pozzi W, Sheffield J, Stefanski R, Cripe D, Pulwarty R, Vogt JV, Nicholson M (2013) Toward global drought early warning capability. *Bull Am Meteorol Soc* 94(6):776–787
- Rahimzadeh Bajgiran P, Darvishsefat AA, Khalili A, Makhdom MF (2008) Using AVHRR-based vegetation indices for drought monitoring in the Northwest of Iran. *J Arid Environ* 72(6):1086–1096
- Raziei T, Saghafian B, Paulo AA, Pereira LS, Bordi I (2009) Spatial patterns and temporal variability of drought in Western Iran. *Water Resour Manag* 23(3):439–455
- Raziei T, Bordi I, Santos Pereira L (2011) An application of GPCC and NCEP/NCAR datasets for drought variability analysis in Iran. *Water Resour Manag* 25(4):1075–1086
- Reichle RH, Koster RD, De Lannoy GJM, Forman BA, Liu Q, Mahanama SPP, Toure A (2011) Assessment and enhancement of MERRA land surface hydrology estimates. *J Clim* 24:6322–6338
- Rienecker MM, Suarez MJ, Gelaro R, Todling R, Bacmeister J, Liu E, Bosilovich MG, Schubert SD, Takacs L, Kim G-K, Bloom S, Chen J, Collins D, Conaty A, da Silva A (2011) MERRA: NASA's modern-era retrospective analysis for research and applications. *J Clim* 24:3624–3648
- Rodell M, Houser PR, Jambor U, Gottschalck J, Mitchell K, Meng C-J, Arsenault K, Cosgrove B, Radakovich J, Bosilovich M, Entin JK, Walker JP, Lohmann D, Toll D (2004) The global land data assimilation system. *Bull Am Meteorol Soc* 85(3):381–394
- Sayari N, Bannayan M, Alizadeh A, Farid A (2013) Using drought indices to assess climate change impacts on drought conditions in the northeast of Iran (case study: Kashafrood basin). *Met Apps* 20: 115–127
- Schneider U, Becker A, Finger P, Meyer-Christoffer A, Rudolf B, Ziese M (2011) GPCC full data reanalysis version 6.0 at 0.5: monthly land-surface precipitation from rain-gauges built on GTS-based and historic data. doi:10.5676/DWD_GPCC/FD_M_V6_050
- Schneider U, Becker A, Finger P, Meyer-Christoffer A, Ziese M, Rudolf B (2014) GPCC's new land surface precipitation climatology based on quality-controlled in situ data and its role in quantifying the global water cycle. *Theor Appl Clim* 115(1–2):15–40
- Sorooshian S, Hsu KL, Gao X, Gupta HV, Imam B, Braithwaite D (2000) Evaluation of PERSIANN system satellite-based estimates of tropical rainfall. *Bull Am Meteorol Soc* 81:2035–2046
- Sorooshian S, AghaKouchak A, Arkin P et al (2011) Advanced concepts on remote sensing of precipitation at multiple scales. *Bull Am Meteorol Soc* 92:1353–1357. doi:10.1175/2011BAMS3158.1
- Tabari H, Abghari H, Hosseinzadeh Talaei P (2012) Temporal trends and spatial characteristics of drought and rainfall in arid and semiarid regions of Iran. *Hydrol Process* 26(22):3351–3361
- Tabari H, Nikbakht J, Hosseinzadeh Talaei P (2013) Hydrological drought assessment in Northwestern Iran based on streamflow drought index (SDI). *Water Resour Manag* 27(1):137–151
- Turk FJ, Rohaly G, Hawkins JD, Smith EA, Grose A, Marzano FS, Mugnai A, Levizzani V (2000) Analysis and assimilation of rainfall from blended SSM/I, TRMM and geostationary satellite data, preprints, 10th Conf. on Satellite Meteorology and Oceanography, Long Beach, CA, Amer. Meteor. Soc., 66–69, (The abstract is available on line at https://ams.confex.com/ams/annual2000/techprogram/paper_147.htm)
- Vicente-Serrano SM (2006) Spatial and temporal analysis of droughts in the Iberian Peninsula (1910–2000). *Hydrol Sci J* 51(1):83–97
- Vicente-Serrano SM, Beguería S, López-Moreno JI (2010) A multiscalar drought index sensitive to global warming: the standardized precipitation evapotranspiration index. *J Clim* 23(7). doi:10.1175/2009JCLI2909
- Wilhite DA, Sivakumar MVK, Wood DA (2000) Early warning systems for drought preparedness and drought management. In: Wilhite DA (ed) Proceedings of an Expert Group Meeting held in Lisbon, Portugal, 5–7 September 2000. World Meteorological Organization, Geneva, 208 pp
- Wilks DS (2006) Statistical methods in the atmospheric sciences, 2nd ed. Academic Press, 627 pp
- Yatagai A, Kamiguchi K, Arakawa O, Hamada A, Yasutomi N, Kitoh A (2012) APHRODITE: constructing a long-term daily gridded precipitation dataset for Asia based on a dense network of rain gauges. *Bull Am Meteorol Soc* 93:1401–1415
- Yi Y, Kimball J, Jones L, Reichle RH, McDonald K (2011) Evaluation of MERRA land surface estimates in preparation for the Soil Moisture Active Passive mission. *J Clim* 24(15):3797–3816